1-1-2016

Ultra-Wideband Radar Based Human Motion Analysis

Zhichong Zhou
University of Denver

Ultra-wideband Radar Based Human Motion Analysis

A Thesis

Presented to

the Faculty of the Daniel Felix Ritchie School of Engineering and Computer Science

University of Denver

---

in Partial Fulfillment

of the Requirements for the Degree

Master of Science

---

by

Zhichong Zhou

June 2016

Advisor: Jun Zhang

Author: Zhichong Zhou
Title: **Ultra-wideband Radar Based Human Motion Analysis**
Advisor: Jun Zhang
Degree Date: June 2016

Abstract

This thesis proposes and investigates two techniques in ultra-wideband (UWB) radar based human motion analysis. The first one is accurate human body landmark detection using UWB radars. The detection is achieved by moving target indication (MTI) and constant false alarm rate detection (CFAR). A new CFAR detection technique is proposed, namely the out-of-band (OB) CFAR detection. In the field experiment, two RF reflective markers are attached to the wrist and elbow of one human arm for reflecting radar signals. It is demonstrated that detection of two markers are feasible and successfully achieved. And our results suggests the OB-CFAR performs better than conventional CFAR in landmark detection. The second technique aims to study on the human motion classification through the exploitation of video and radar data, respectively. Motion history image (MHI) and Hu moment method are applied to extract temporal features from video clips. Principal component analysis (PCA) is used to obtain radar detection signitures. We use k-means clusters to quantize the observation feature vectors. Hidden Markov models (HMMs) are trained with the features extracted from both video and radar data to discern the motion types. Experiment results indicate that the proposed approach can provide improved performance in distinguishing fall motions from other motions such as sitting.

Acknowledgements

I would like to thank Dr. Jason Zhang for all his help, patience and support throughout this research. I would like to thank my family and friends who helped me in many ways to bring this thesis to a successful completion. I would like to thank all the members in the lab for all their help and explanations during the thesis development.

Table of Contents

List of Figures

Chapter 1

Introduction

1.1 Motivation

Healthcare for aging population has been one of the greatest concerns for mpdern societies around the global. Aged persons, especially those who have heart diseases, hypertension, diabetes and stroke, easily suffer from emergencies such as sudden falls. Many techniques are developed to respond to these challenges, such as visual imaging techiques. However the visional line-of-sight could be probably blocked by indoor furnishings or other human obstacles. Ultra-wideband (UWB) eletromagnetic waves are able to penetrate through many types of materials and detect human motions with a high resolution. Therefore, UWB radars show advantages in human motion detecting. Previous work on video based motion detection makes it possible to classify different motions through machine learning. One of the questions in UWB radar based real-time human activities monitering is that, can UWB radar based approaches generate comparable or better performance compared with vision based approaches? This thesis investigates the potential benefits that UWB radars can bring to human motion detection and classification.

1.2 Literature Review

Human motion measuring and reasoning are stimulated by a wide spectrum of applications, and is able to satisfy the social needs for intelligent systems in a wide range of implantations in healthcare, biometrics, homeland security, sports and robotics. In [1], sensors that applied for human movement, gait and posture analysis are summarized. It discussed electro-optical technique and video analysis but for these types of sensing methods the authors have concerned on the matters of restricted applicable scenarios, i.e., only for controlled laboratory environment, and apparently, privacy. Electrical sensors, such as gyroscope, accelerometer, flexible angular sensor, and sensing systems such as electromagnetic tracking system have been widely used to solve such problems caused by visual-based methods, however, the main tasks of those systems are still signal processing, feature extraction and the integral performance of these systems. In the last decade, the UWB radar and radio technologies [2, 3] and their implementations in diverse critical fields were greatly developed. A beneficial characteristic of the UWB radio frequency sensing that distinguishes it from other sensors is the capability in penetrating obstacles, such as walls, furnitures or even human beings. Accordingly, through-wall sensing becomes a significant area of investigation for UWB radar implementations [2,4–10]. Movement detection [11, 12] and Human detection [5, 6, 9–11, 13] are other areas that with the applications of UWB radars, when combining with the capability to see through the wall, UWB radars provide estimable sensing modalities in security surveillance. The biomedical applications of UWB radars is reviewed in [14], including arterial pulsation tracing, medical imaging, pregnancy monitoring and cardiac motion evaluation. As a type of sensing pattern with high range resolution and penetration capability, the UWB radar plays substantial roll in biomedical applications. In [12, 15–21], the UWB radar based vital physiological signal monitoring techniques are further evaluated and developed, including respiration motion and cardiac motion from single

and multiple subjects. [21, 22] investigates the method for gait human motion gait analysis and quantificaiton, which explains that, although the analysis on human gait motion is now recognized as financially reimbursable and clinically useful in conditions, its medical application is most likely to be hindered by the time inefficiency and costs required to perform and to interprete it. The motion or gait data need to be interpreted efficiently and effectively by a class of modeling, statistical and artificial intelligence methods. The more plicated human motion analysis, which aims at fetching necessary information from UWB radar echos, is further evoluted recently based on technical developments in radar signal feature and human activity characteristics extraction and machine learning [7,16,18,23–26]. UWB synthetic aperture radar (SAR) techniques provide another possible way to image and analyze moving target, and were successfully presented in [2, 8, 9, 25, 27, 28]. There are several other biomedical applications of UWB radars including transfer function estimation of vocal tract filter [29], arterial stiffness measuring, [30], human arm muscle characterization [31], etc.

Differentiate from the existing UWB radar based techniques introduced above, in Chapter 2 we investigate the practicability of UWB radar based human body landmark detecting, which uses amplified radar echos from reflectable spherical markers attached on human body as landmarks. This research work presented is aiming at exploring the feasibility of sophisticated sensing method and signal process methodologies in accurate human motion detection. Specifically, a UWB radar is applied to transmit and receive signals for detecting, radio frequency(RF) reflective makers are attached as human body landmarks. As the reflectivity properties of human body, clothing, markers and clutters are quite different [32], distinction of the markers from background is feasible, detection and location of the markers can be successfully realized. The radar echos are then processed using moving target indication (MTI) and Doppler filter bank. Then targets are detected and separated using the

constant false alarm rate (CFAR) detection techniques. To further separate the radar echos from the targets, other objects such as clothes, we propose an advanced CFAR detector, namely the out-of-band CFAR (OB-CFAR), which utilizes the signal energy in the frequency band that divided by Doppler filter banks to determine the CFAR threshold.

In this thesis, Chapter 3 discusses the UWB radar based human motion classification. Falls are the leading cause of injurious hospitalization for elderly. They have attracted significant interests to develop new techniques for prompt fall detection which saves lives and leads to effective treatments and cost reduction [33] [34]. Different sensing modalities have been proposed for this pursose, including intertial measurement unit-based wearable devices, video camera, and radar [35] [36] . Wearable devices have shortcomings that they are intrusive, easily broken and must be worn or carried. Video provides a non-invasive modality for motion classification and fall detection. In the field of human motion research, video based classification is widely used with the advantage of direct perceiving and simplicity. Recognition of human motion within a video is considered a key problem of computer vision. Vision based approaches generally use videos or images to analyze motion features of a human body, and distinguish features of fall activities from those of non-falls to achieve the function of fall detection.

Motion capture systems provide accurate three-dimensional (3-D) information of different human motions such as walking, running and crawling [37]. Kinect sonsor is one such type of sensors with an attractive price [38]. However, there are limitations of vision-based approaches in the real life applications, in additionnal to privacy concerns, line-of-sight can be easily obstructed by walls and furniture. The Kinect sensor is sensitive to external infrared sources which can significantly influence the captured depth of the video images. Furthermore, the visual image data are sensitive to cluttered backgrounds. On the other hand, radar carries great potential

to be one of the leading technologies due to its advantages of non-obstructive illumination, insensitivity to lighting conditions, privacy preservation and safety [35] [39]. In particular, for UWB radars that are considered in this thesis, the range-direction occupancy of a target can be observed. This provides useful features about the spatial distribution of a target for human motion classification and fall detection [40]. In addition, radar can obtain indirect but meaningful characteristics representing the moving trajectories [41].

In Chapter 3, the above two different sensing modalities for fall detection are examined and compared. A Kinect sensor is utilized to record human motions using RGB images, whereas a UWB radar is employed in the same experimental configuration to collect radar echo signals from human motions. The video and radar data are then used to examine and compare for their motion classification and fall detection performance.

1.3 Thesis Organization

This thesis comprises 5 chapters which are organized as follows. Chapter 2 introduces the basic concept and characteristics of UWB radar and discusses the UWB radar based human body landmark detection including radar model establishing, moving target identification. An OB-CFAR method is introduced to detect the landmarks. In Chapter 3, the motion history image (MHI) method is used to describe motion patterns, and the Hu Moments are exploited to extract image features. In addition, Principal Component Analysis (PCA) is used to reduce the dimension of radar data, and the k-means method is applied to perform vector quantization on both vision and radar features. Finally the Hidden Markov Models (HMMs) are employed to build two motion models. Chapter 3 also presents the experimental results with discussion. At last, concluding remarks are presented in Chapter 4.

Chapter 2

UWB Radar Based Human Body Landmark Detection

2.1 Introduction to UWB Radars

Ultra-wideband (UWB) is a prefered signaling choice for high accuracy localization in short to medium distances due to its high range and time resolution [42]. It is also well-suited for short range and low data rate communications.

In general, a UWB signal is defined to be a signal with a fractional bandwidth of larger than 20% and/or an absolute bandwidth of at least 500 MHz. The most important feature of UWB signals is that they have a much wider frequency band than conventional signals. Therefore, certain regulations are imposed on systems transmitting UWB signals in different countries [42]. The common definitions for the bandwidths of UWB signals are as follows: The difference between the upper frequency of 10 dB emission point and the lower frequency of 10 dB emission point represents the absolute bandwidth. Based on this criteria, a signal can be classified into narrowband, wideband, or ultra-wideband. A signal with bandwidth greater than 500 MHz or greater than 20% of the carrier frequency is characterized as ultra-

wideband signals. Due to such large bandwidth, UWB signals have a very fine range and time resolution [43], thus being ideal for precision ranging and tracking applications. UWB signals have very low power over the frequency band and thus donot create interference level of existing communication services. Also due to their large bandwidth, UWB signals are very difficult to jam. A UWB radar system generates and transmits short pulses and the electromagnetic wave travels through the propagation channel to the target. In this section, technical details of the Pulson 410 Monostatic Radar Module (P410 MRM) are presented. P410 MRM is a monostatic UWB radar platform and can perform band-pass filtering, motion filtering, and constant false alarm rate (CFAR) target detection on the raw scan data. The processed data is provided to the MRM reconfiguration and evaluation tool (RET) for display and logging. The user has the option of applying different types of filters on the radar data. A UWB Radar system configuration is shown in Figure 2.1.

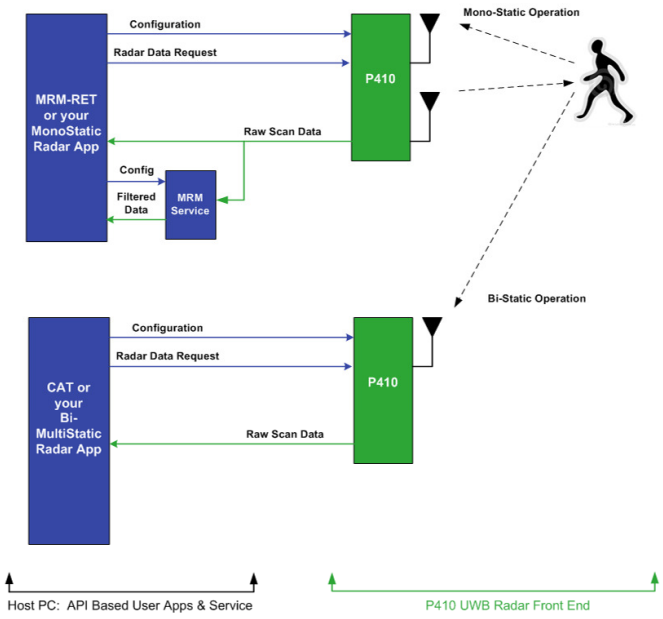

Figure 2.1: P410 MRM UWB sensing configuration.

There are some advantages of the P410 MRM such as very good performance in high multipath and high clutter environments, coherent signal processing (which extends the operating range at very low signal power levels), and the availability of seven separate channels. Moreover, the P410 MRM provides raw scans for post processing and two user-configurable antenna ports for dual antenna operation.

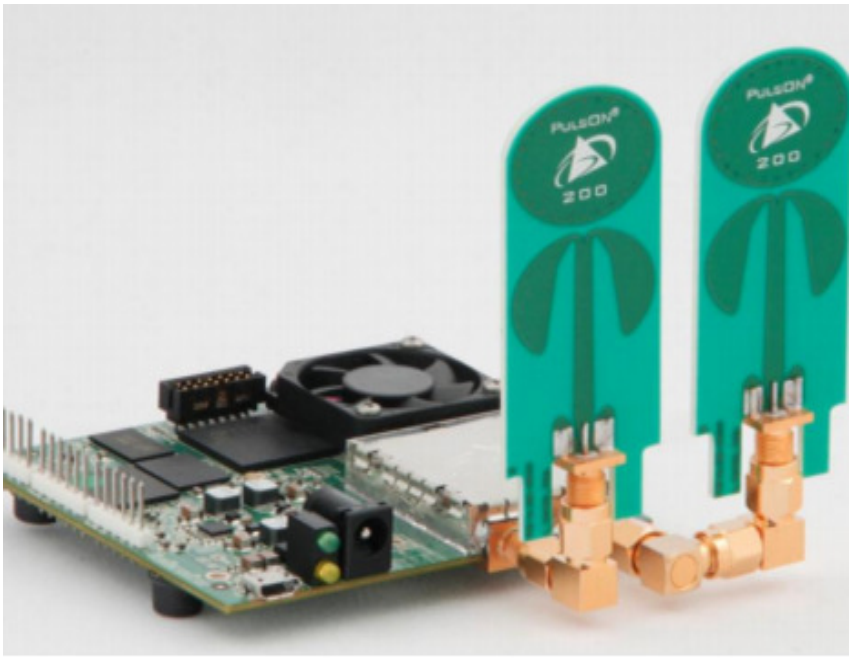

Figure 2.2: Time Domain P410 UWB radar device.

In our experiments, P410 MRMs are employed. The P410 MRM is a monostatic radar platform with frequency centering at 4.3 GHz providing over 2 GHz of radio frequency(RF) bandwidth . Each radar sensor (P410 MRM) has a transmitter and an UWB receiver, the main function of which are emitting and receiving signals. Different code channels are used by radar sensors to prevent interference. In addition, the UWB radar has an scanning phase in a duration of 100ns, it refers to determine signals reflected from moving objects. The UWB pulses are sent from the radar sensors in trains by the transmitter antenna and the echos are collected

by the receiver. P410 MRM UWB sensors provide raw signal, researchers obtain the information of moving targets they need from raw signal using motion filters. However, in some cases, the conventional motion filtered data may not be sufficient or convincing to locate the targets precisely since there can be much useless information, according to the high resolution of UWB signals which are derived from the reflections from other objects or reflectable surfaces in the environment. Therefore, we invent a motion filtering method, as explained in the next section.

2.2 Radar Signal Modeling

Detection of human behavior with radar relies on motion detection. Human cause changes in frequency, phase and time of arrival [44]. The radio frequency (RF) band of the UWB radar is 3.1 GHz to 5.3 GHz. The kth pulse transmitted radar signal is denoted as $s_k(t)$ and its duration is t_r. The sampled signal vector is denoted as $\mathbf{s}_k = [s_{k,1}...s_{k,l}...s_{k,L}]^T$, where $s_{k,l} = s_k(lt_s + (k-1)t_{pr}), Lt_s = t_r$, t_s is the sampling interval, and $(.)^T$ denotes vetor or matrix transpose. Concatenating vectors $s_k, k = 1, 2..., K$, to form a $L \times K$ received signal matrix $\mathbf{S} = [\mathbf{s}_1...\mathbf{s}_k...\mathbf{s}_K]$. A motion filter is firstly applied to obtain the target change detection among the data. The filtered radar signal is expressed as:

$$\mathbf{r}_k = [s_{k,2} - s_{k,1}, ..., s_{k,L} - s_{k,L-1}]^T. \tag{2.1}$$

In such case, we rebuild the filtered radar signal matrix as $R = [\mathbf{r}_1, \mathbf{r}_2, ..., \mathbf{r}_K]$. Figure 3.13 shows the filtered result for falling, and Figure 3.14 for sitting.

In this thesis, the transmission waveform of a single pulse of the UWB radar is given by

$$y(t) = \begin{cases} x(t) & 0 \leq t < T_P \\ 0 & \text{otherwise} \end{cases}$$

where $x(t)$ denotes the UWB radar pulse waveform and T_P is the duration of the pulse. The UWB radar pulse waveform is shown in Figure 2.3. Thus if K pulses are transmitted to form a pulse train, the pulse train can be described as,

$$y_{tr}(t) = \sum_{k=1}^{K} y(t - (k-1)T_{PRI}) \quad k = 1, 2, ..., K, \tag{2.2}$$

where T_{PRI} is the pulse repetition interval (PRI).

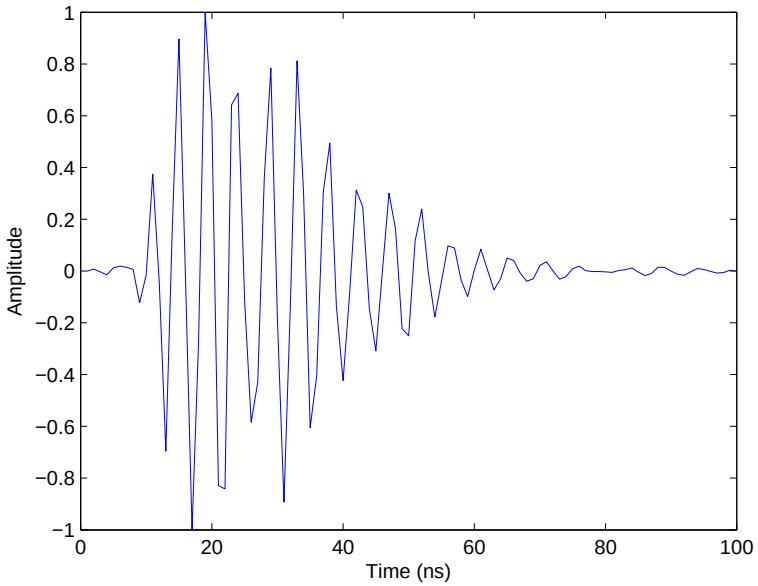

Figure 2.3: The UWB radar pulse waveform.

Assuming the received radar signals corresponding to the kth transmitted pulse as $r_k(t)$ with a duration as T_r. Sample the signals in time domain, we denote the received signal vector as $\mathbf{r}_k = [r_{k,1} \ \cdots r_{k,l} \ \cdots r_{k,L}]^T$, where $r_{k,l} = r_k(lT_s)$ with $LT_s = T_r$, T_s is the sampling period, and T represents matrix transpose. Concatenating

vectors $\mathbf{r}_k, k = 1, \cdots, K$, a $L \times K$ matrix is given by $\mathbf{R} = [\mathbf{r}_1 \ \cdots \ \mathbf{r}_k \ \cdots \ \mathbf{r}_K]$ to represent the received signals. We also denote $\mathbf{R} = [\boldsymbol{\gamma}_1 \ \cdots \ \boldsymbol{\gamma}_l \ \cdots \ \boldsymbol{\gamma}_L]^T$, where in this expression $\boldsymbol{\gamma}_l^T$ is the lth row of $\mathbf{R}$.

The column vectors in the data matrix $\mathbf{R}$, $\mathbf{r}_k$, indicates the radar echoic vector in the fast time domain (l-domain) mapping the kth pulse. The row vectors in the data matrix $\mathbf{R}$, $\boldsymbol{\gamma}_l^T$, represents the radar echoic vector in slow time domain (k-domian) corresponding to the index l. This matrix is aiming at catching the moving targets and identifying the specific range between radar and targets, based on this matrix, all our consequential signal processing is carried out. Figure 2.4 shows an example of the raw data matrix $\mathbf{R}$. As we can see, although the UWB radar has a very fine range resolution, it is impossible to separate the targets from the clutter, noise and interference without further processing.

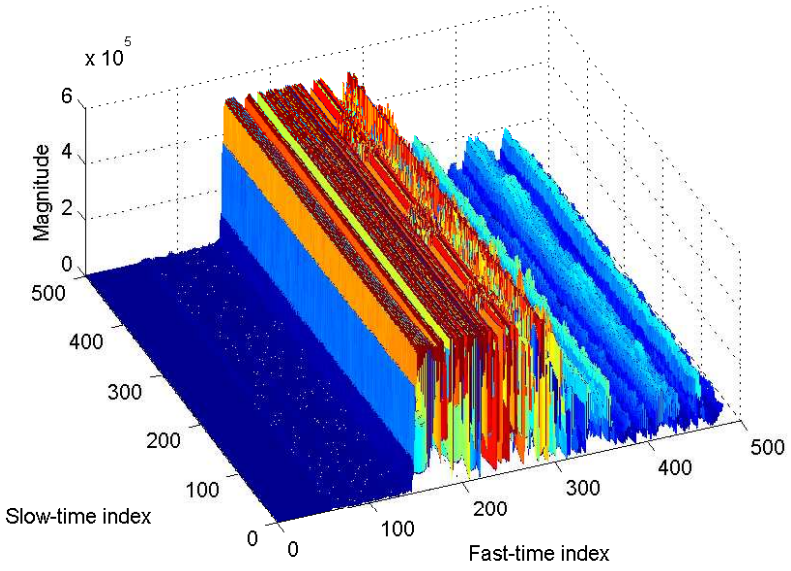

Figure 2.4: An example of the received data matrix $\mathbf{R}$.

2.3 Moving Target Identification

MTI processing is applied in slow time domain performing as a filter to suppress clutter components in the radar echos, which is aiming at reducing and eliminating the static radar clutters, since only the varying adjacent pulses transimit useful information from moving targets. Traditionally, we simply use two pulse canceller to reject clutters. However there are many other pulse cancellers have been developed as motion filters. It is necessary to compare their performances and decide which canceller is more proper in our case. Figure 2.5 displays the diagrams and the working machanisms of two and three pulse cancellers. The diagram of a four pulse canceller is given by Figure 2.6. Figure 2.7 shows a comparison in frequency responds among two, three and four pulse cancellers.

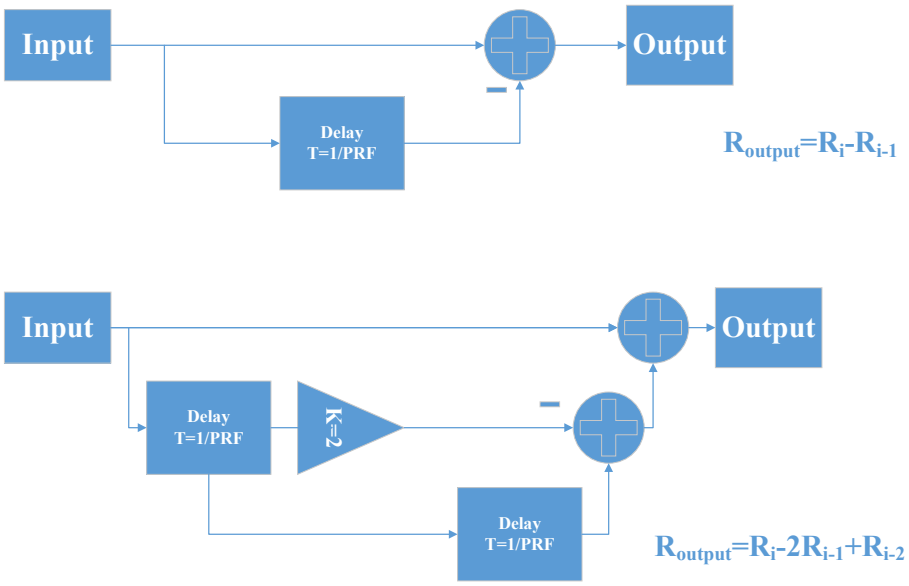

Figure 2.5: Diagram of two pulse canceller and three pulse canceler

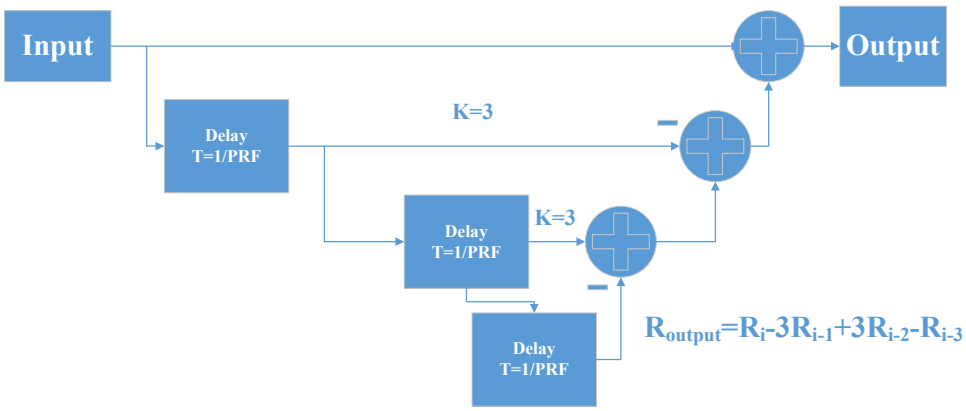

Figure 2.6: Diagram of four pulse canceler.

As we can see in Figure 2.7, the four pulse canceller shows an excellent manifestation in eliminating low frequency subjects as a bandpass filter. Previous studies [45] also show that the four pulse canceller performs better in effective number reduction of independent samples from static radar clutters. A four pulse canceller which is regarded as a motion filter is applied on the data matrix $\mathbf{R}$ to remove the static clutters and extract moving target features from the radar echos. The discrete impulse response of the canceller can be formulated by $h(k) = \delta(k) - 3\delta(k-1) + 3\delta(k-2) - \delta(k-3)$, where $\delta(\cdot)$ is the Kronecker delta function. Applying the pulse canceller to row vectors $\boldsymbol{\gamma}_l$, the resulting signal is given by $\boldsymbol{\theta}_l = \boldsymbol{\gamma}_l \otimes \mathbf{h}(k)$, where $\otimes$ represents convolution operation.

The static clutters are basically dispelled by the pulse canceller, and the radar echos resulted from moving targets are preserved for next processing step. Figure

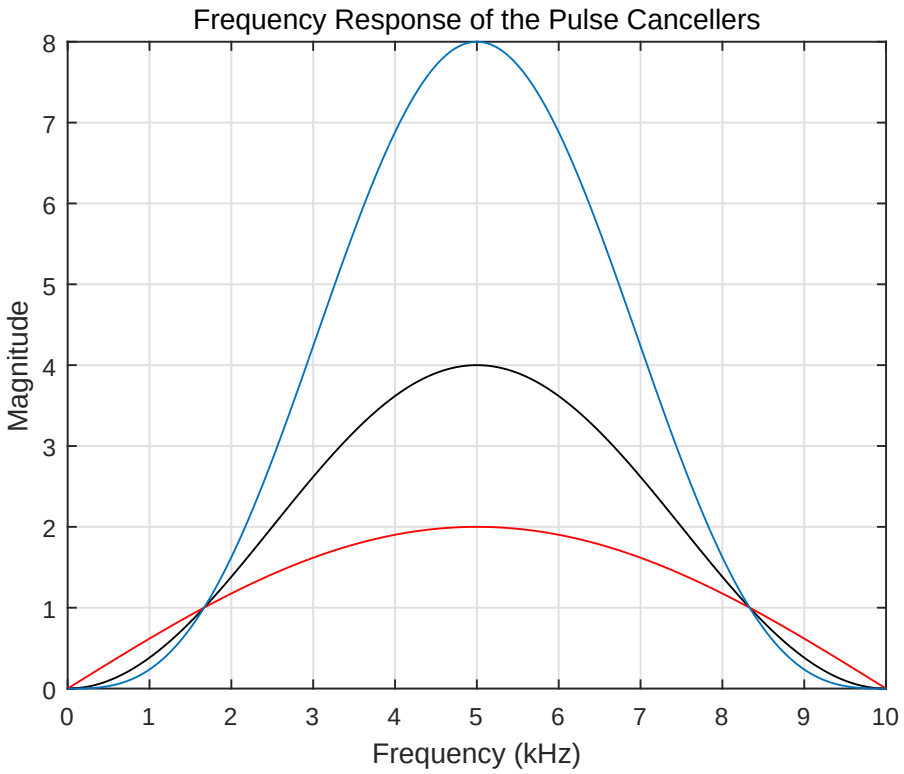

Figure 2.7: Frequency responds of the pulse cancellers

2.8 provides an example of the motion filtering performance.

The above convolution on each $\boldsymbol{\gamma}_l$ transform the data matrix $\mathbf{R}$ into a new data matrix $\boldsymbol{\Theta} = [\boldsymbol{\theta}_1 \ \cdots \ \boldsymbol{\theta}_l \ \cdots \boldsymbol{\theta}_L]^T$.

2.4 Out-of-Band CFAR Detection

2.4.1 N-point Doppler Filter Bank:

The UWB radar has a large range of operating band, in order to further dispose the clutters as well as noise, we divide the Doppler frequency band into narrow sub-bands. Ideally there should be no overlap in sub-band frequency characteristics. In this case Doppler filter bank is utilized. The noise bandwidth of the Doppler filters

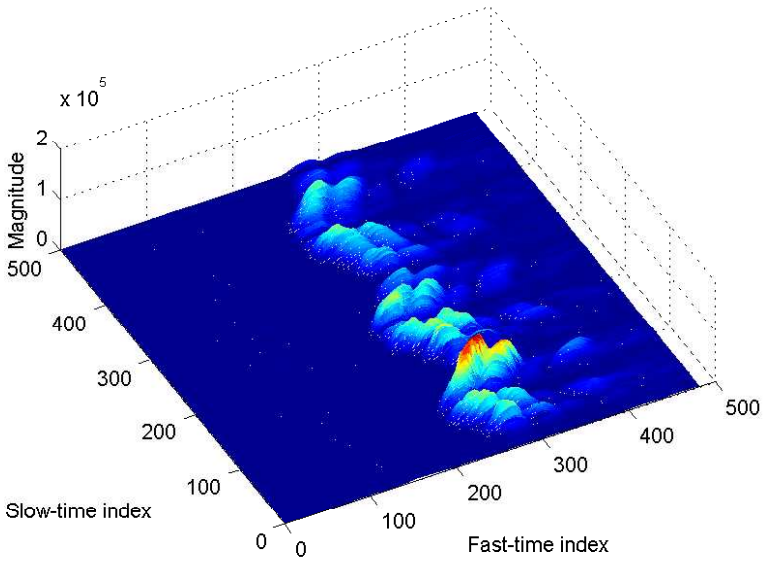

Figure 2.8: The resulting data matrix $\mathbf{\Theta}$ after motion filtering.

is much smaller compared to that of the radar's total bandwidth, it helps us improve the signal noise ratio(SNR). This Doppler filter bank can be generated by FIR filter. The ideal FIR digital filter should have the characteristics as

$$H_k(f) = \begin{cases} 1, & |f - \frac{k}{N}F_{pr}| \leq \frac{1}{N}F_{pr}, \\ 0, & \frac{1}{N} < f - \frac{k}{N}F_{pr} < \frac{1}{2}F_{pr}, \end{cases} \tag{2.3}$$

where N is the number of filters in this FIR filter bank; k denotes the kth filter.

Suppose that $k = 0$, which means the 0th filter in a N-point filter bank , in this case,

$$H_0(f) = \begin{cases} 1, & |f| \leq \frac{1}{N}f_r, \\ 0, & \frac{1}{N} < f < \frac{1}{2}f_r, \end{cases} \tag{2.4}$$

According to the Fourier Transform, the impulse response for this filter is,

$$h_0(n) = \int_{-\frac{1}{N}f_r}^{\frac{1}{N}f_r} e^{j2\pi f(n-\frac{N-1}{2})} df \tag{2.5}$$

Figure 2.9 shows the plot of 0th Doppler filter in the bank.

We utilize a N-point Doppler filter bank, which is formed by N bandpass filters on different frequency bands for processing the received signals in the slow time domain. The outputs from the filter bank will be N $L \times K$ matrices $\mathbf{\Omega}_n$, $n = 1, \cdots, N$ with $\mathbf{\Omega}_n$ containing received radar signals in the nth frequency band. The frequency response $H_n(f)$ for the nth Doppler filter is given by

$$H_n(f) = \frac{\sin(\pi N(f/F_{PRI} + n/N))}{\sin(\pi(f/F_{PRI} + n/N))},$$

where, F_{PRI} is the pulse repetition frequency. We denote the outputs from the nth Doppler filter as $\mathbf{\Omega}_n = [\boldsymbol{\omega}_{n,1}\ \boldsymbol{\omega}_{n,2}\ \cdots\ \boldsymbol{\omega}_{n,L}]^T$ with $\boldsymbol{\omega}_{n,l} = \mathcal{F}^{-1}[\mathcal{F}(\boldsymbol{\theta}_l)H_n(f)]$, where $\mathcal{F}$ denotes discrete Fourier transform.

2.4.2 OB-CFAR Detection

The OB-CFAR detector is designed in the following methodology. For each given fast time index l, which is the row index in the radar matrix, the Doppler frequency band with the maximum signal energy $n_l^{\max}$ can be determined as $n_l^{\max} = \max_n \|\boldsymbol{\omega}_{n,l}\|_2$, where $\|\cdot\|_2$ is the ℓ_2 norm. Concatenating the vectors $\boldsymbol{\omega}_{n_l^{\max},l}$, $l = 1, \cdots, L$, we define the *in-band signal matrix* as $\Psi^{\mathrm{IB}} \triangleq \left[\boldsymbol{\omega}_{n_1^{\max},1}\, \boldsymbol{\omega}_{n_2^{\max},2}\, \cdots\, \boldsymbol{\omega}_{n_L^{\max},L}\right]^T$, the lth row of the matrix represents the signal from the Doppler frequency bank where the maximum signal energy appears in each row l. The *out-of-band signal matrix* is defined as $\mathbf{\Psi}^{\mathrm{OB}} \triangleq \mathbf{\Psi} - \mathbf{\Psi}^{\mathrm{IB}}$. The cell averaging CFAR detection is ameliorated to use the out-of-band signals in $\mathbf{\Psi}_{\mathrm{OB}}$ to better describe the noise and better distinguish the targets from other objects. The resulting out-of-band

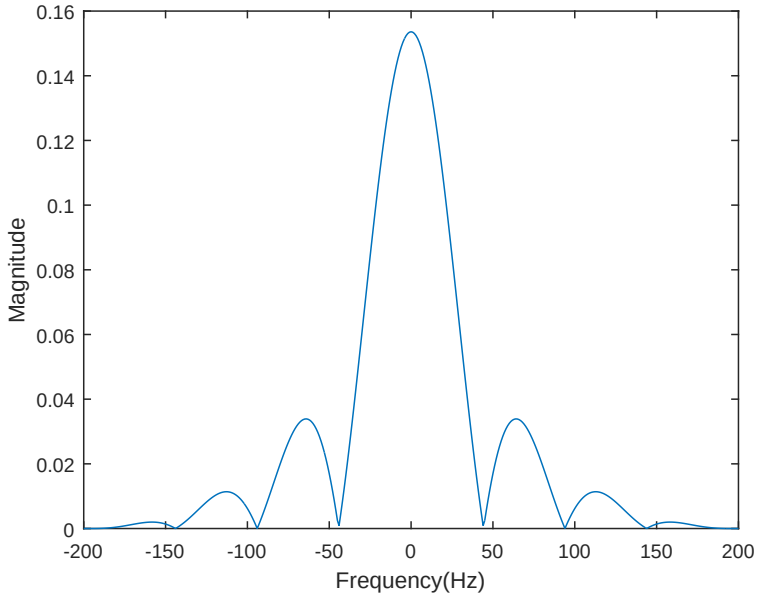

Figure 2.9: An example of 0th channel in Doppler filter bank.

CFAR (OB-CFAR) detecting methodology can be formulated as following. We denote the (l,k)th element $\mathbf{\Psi}_{\mathrm{OB}}$ as $\psi_{l,k}^{\mathrm{OB}}$. For the (l,k)th element, as denoted as "cell", in the matrix $\mathbf{\Psi}$, the CFAR threshold $\chi_{l,k}$, is given by $\chi_{l,k} = \eta\vartheta_{l,k}$. Where $\vartheta_{l,k} = \frac{1}{N_{\mathrm{tr}}}\sum_{l\in\mathcal{L}_l^{\mathrm{tr}}}|\psi_{l,k}^{\mathrm{OB}}|^2$ is the noise power estimation, and $\mathcal{L}_l^{\mathrm{tr}}$ is the index of the training cells, and the N_{tr} denotes the size of the $\mathcal{L}_l^{\mathrm{tr}}$ and describes the length of training cells. In general, $\mathcal{L}_l^{\mathrm{tr}}$ consists of the indices of the leading and lagging training cells for cell (l,k) in the range domain. The threshold factor η is defined by

$$\eta = N_{\mathrm{tr}}(P_{fa}^{-1/N_{\mathrm{tr}}} - 1),$$

where P_{fa} is the desired false alarm rate which is man-made. In our experiments, P_{fa} is set at value 10^{-2}.

2.5 OB-CFAR Detection Results

Applying our OB-CFAR detector on $\mathbf{\Psi}$ in the fast time(range) domain for detecting multiple targets after motion filtering, the targets are better distinguished from the background. Figure 2.10 shows the detection results when the OB-CFAR detector is used for detection, and Figure 2.11 shows the results that a conventional CFAR detector is applied. Those figures indicate that the OB-CFAR achieves better performance in detecting and separating the two reflectors.

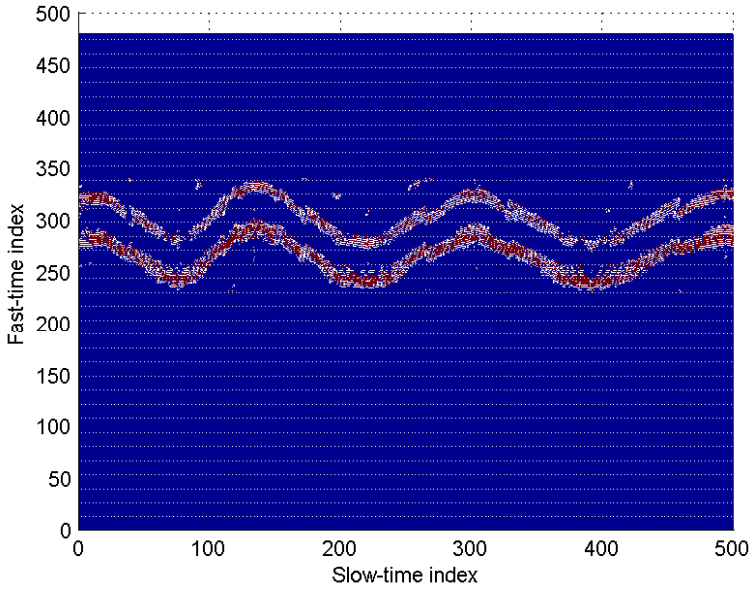

Figure 2.10: OB-CFAR detection results of two markers on a moving arm.

2.6 Human Body Landmark Detection Results

We designed two experiments to evaluate and validate our designs and proposed approach, there are two spherical markers that are made with metallic foils, are considered as our moving targets, In Experiment I, those two markers are attached to a ruler, and in Experiment II, they are attached respectively to the elbow and

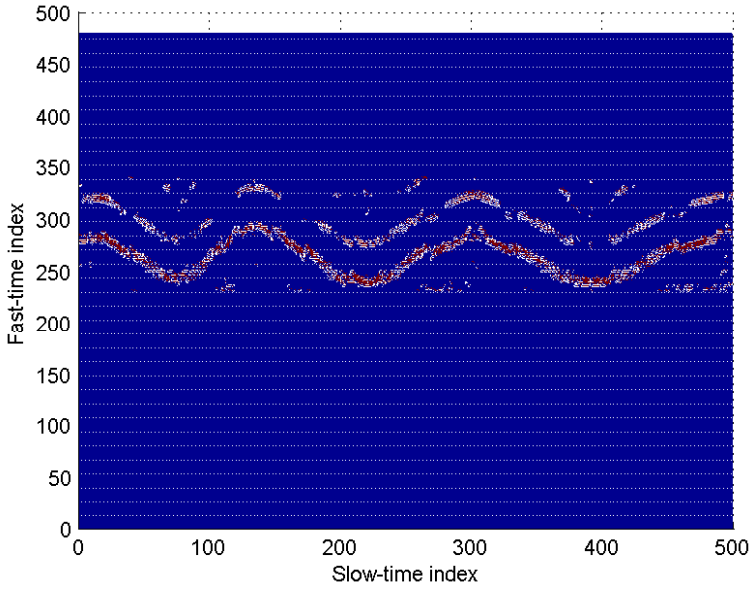

Figure 2.11: Conventional CFAR detection results of two markers on a moving arm.

wrist of a human's arm. The UWB radar used in these experiments transmits waveforms from 3.1 GHz to 5.3 GHz, centering at 4.3 GHz. The UWB radar is fixed on a suspended beam with its antennas facing the ground, which makes the boresight direction of the antenna perpendicular to the ground. In Experiment I, a person holding the ruler stands right beneath the radar moves the ruler back and forth repetively to the radar. In order to better observe the changes in range, we intended to keep the moving ruler and the antenna aperture in a two-dimensional (2D) plane, in which case the two markers remain in the $x-y$ plane. In Experiment II, the two reflective markers are attached to the elbow and wrist of a moving arm. The subject stands still beneath the radar and waves his arm up and down remaining his arm and the apertures in the same plane as well. The experimental scenarios for both experiments are shown in Figure 2.12.

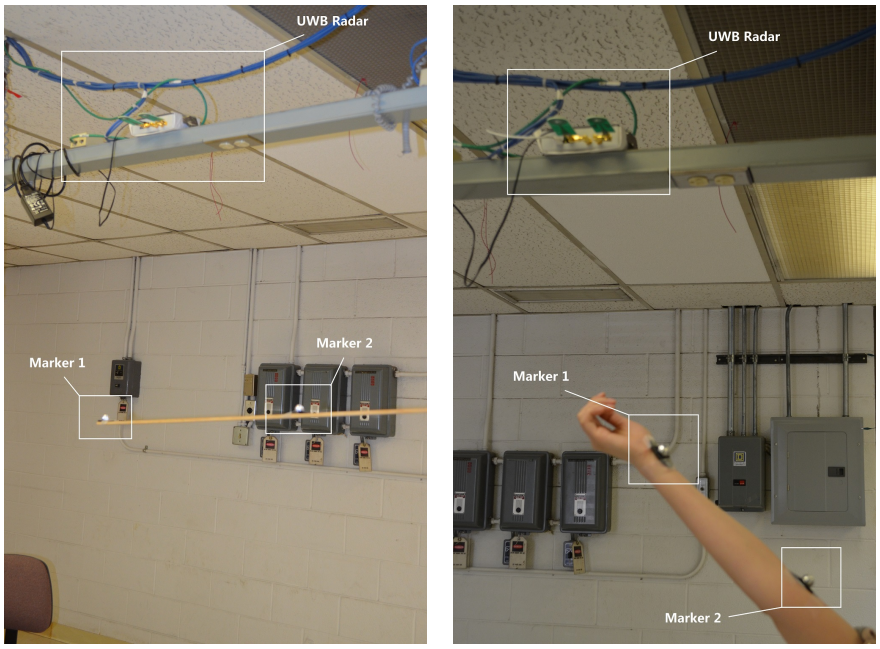

Figure 2.12: Scenarios for Experiment I with a moving ruler (left), and Experiment II with a moving arm (right).

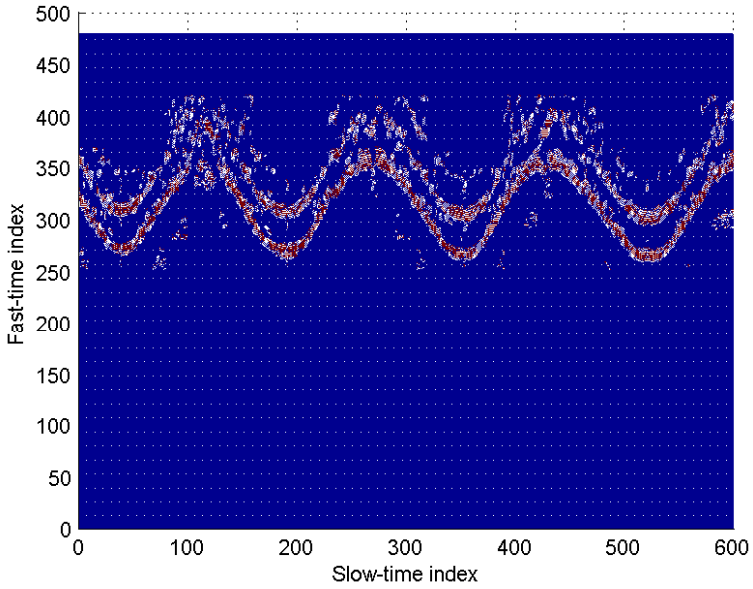

Figure 2.13: OB-CFAR detection results of two reflective markers on a ruler in Experiment I

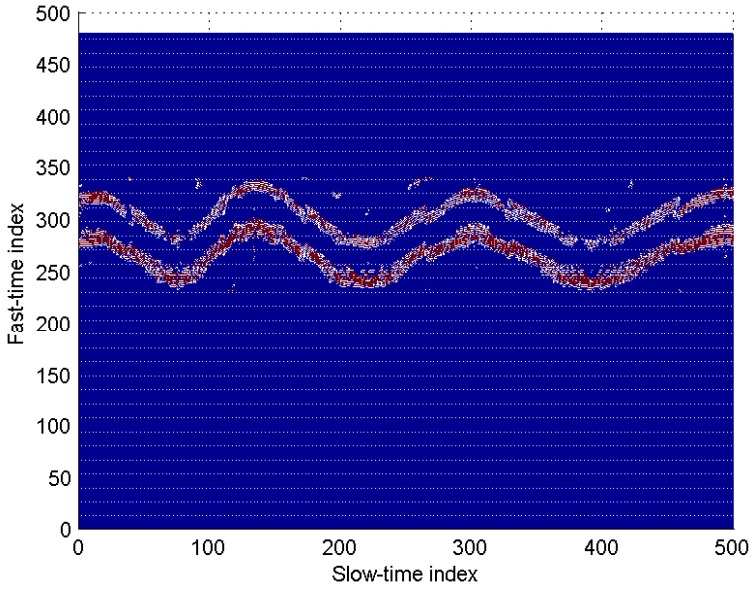

Figure 2.14: OB-CFAR detection results of two reflective markers on a moving arm in Experiment II.

Chapter 3

UWB Radar Based Motion Classification

Motion detection and classification is a typical way to recognize human motion by utilizing various sensor readings. Most existing studies extract human motion features from micro-Doppler signitures of radar signals. The radar signals are used to characterize human motion features [46] in the time-frequency domain. In this thesis, we investigate a UWB based classification technique to distinguish different types of human motions, and compare its performance with an image based approach. Figure 3.1 provides the process diagram of image and radar based human motion classification.

3.1 UWB Radar Based Signal Characteristics with Human Motions

3.1.1 Single-person Motions

The experiments of single person fall detection are mainly aimed at distinguishing fall from sit and other possible motions. The subjects perform different motions

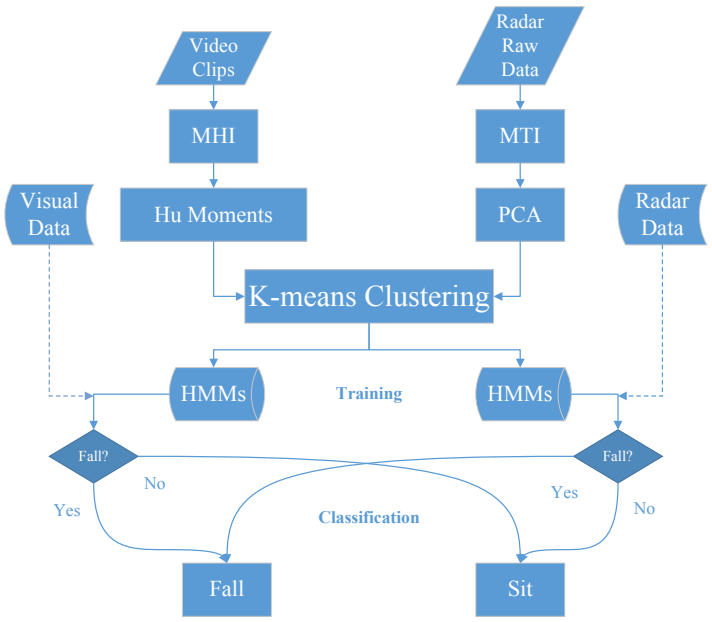

Figure 3.1: Diagram of human motion classification process.

in front of the radar sensor, and the radar returns are collected and shown in Figure 3.2 and 3.3.

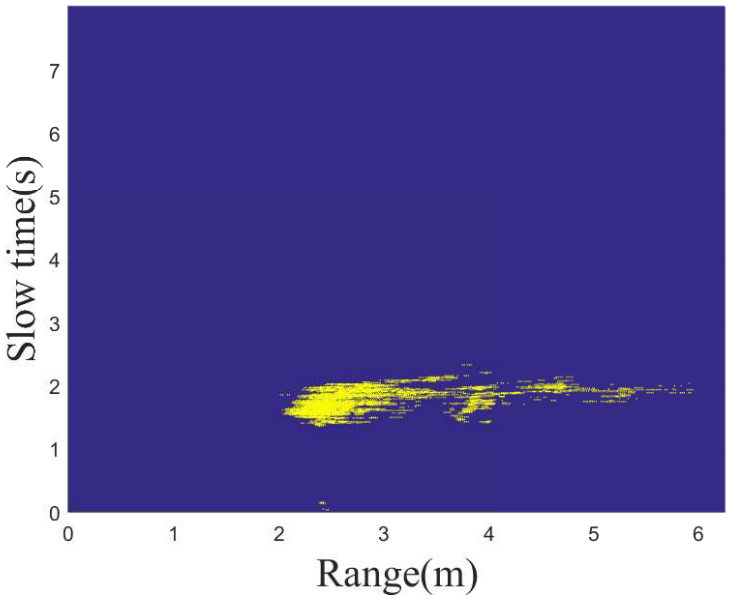

Figure 3.2: The radar signal corresponding to a single-person falling

Figure 3.2 is the radar signal corresponding to fall motion. It has a approximate range extension of 3 meters. In Figure 3.3, which corresponds to a single person sit motion, the range extension is only around 1 meters. This difference in range changes gives a distinguishing characteristic of fall and sit motions.

3.1.2 Multi-Person Motions

In many cases, multiple persons can appear in the suvaillance scene. Experiments are conducted to investigate whether the UWB radar can distinguish motions from two persons. One of the subjects sits down and gets up repeatively while the other walks around the first person. Figure 3.4 is the layout of this experiment. Figure 3.6 shows the collected radar signal reflected from the two subjects performing sitting and walking, respectively.

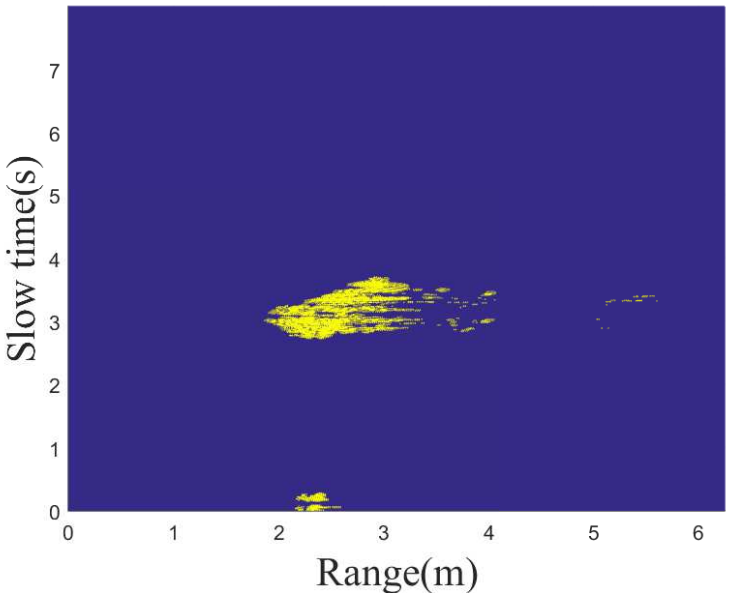

Figure 3.3: The radar signal corresponding to a single-person sitting.

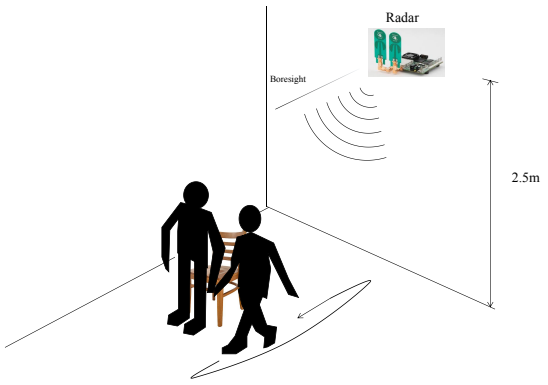

Figure 3.4: The experiment layout of multi-person motions.

Figure 3.5: The experiment scenario of multi-person motions.

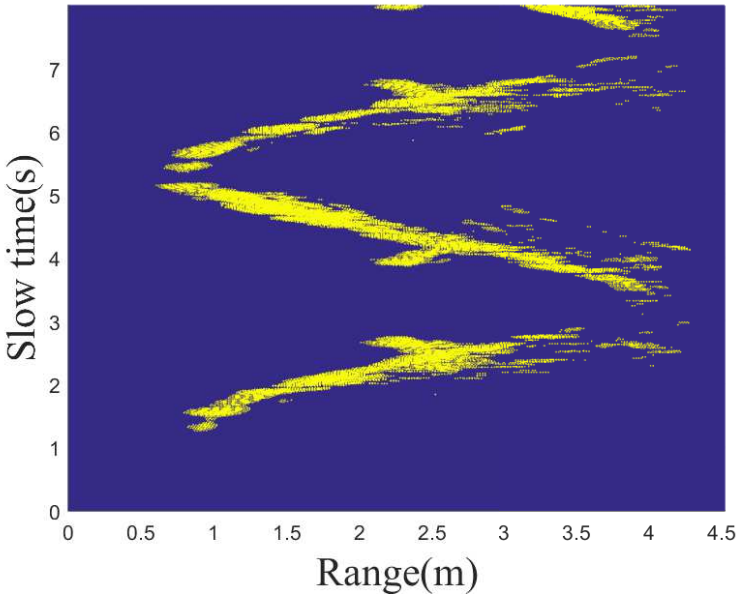

Figure 3.6: The radar signal corresponding to the scenario where two subjects performs walking and sitting, respectively.

Figure 3.6 successfully shows the signal characteristics corresponding to walking and sitting. In order to investigate the difference between walking and falling, another experiment was designed as, one subject falls down while the other passing by. Figure 3.7 is the layout of this experiment. Figure 3.8 clearly shows that there

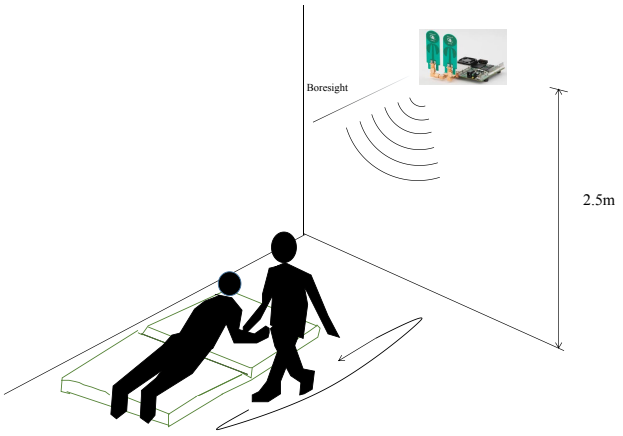

Figure 3.7: Experiment layout for one person parallelly falls with another one walks by.

is a falling trajectory parallel to the walking trail around range of 2.5 to 4m and slow time of 3-4s.

3.1.3 Multi-Radar Human Motion

We utilize two radar sensors to observe experiments from different angles to provide omni-directional radar signal retures. We design and conduct two experiments to show the benefits of multi-radar observation and detection in the first experiment, the subject stands and sits repeatively. Two radars are placed on different location with their boresights being orthogonal to each other. Figure 3.9 shows the layout of multi-radar experiments.

Figure 3.10 show that different radar provides different radar images with different range extension for the same motion. In the second experiment, We adjust

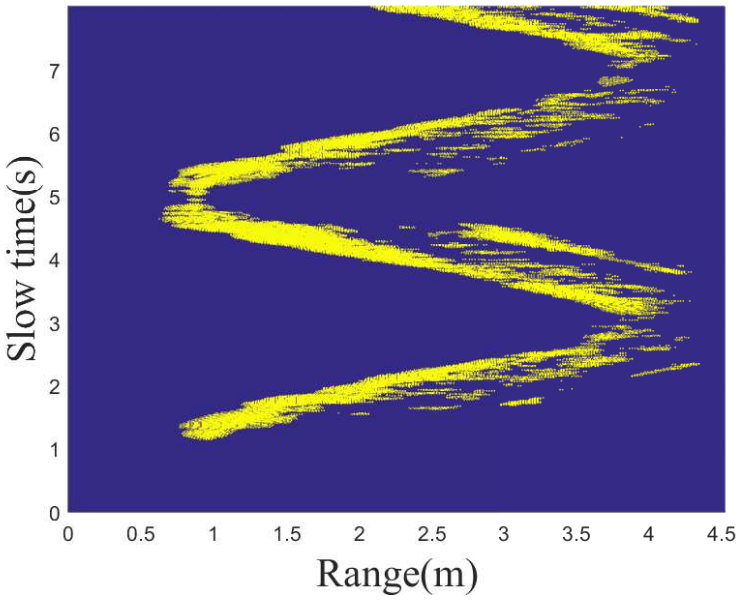

Figure 3.8: One person parallelly falls with another one walks by.

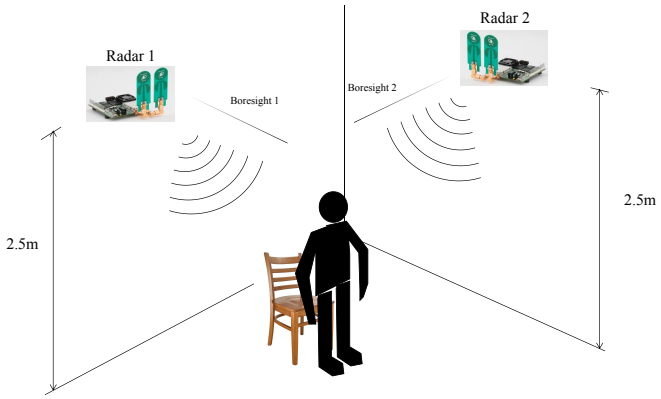

Figure 3.9: Multi-radar experiments layout.

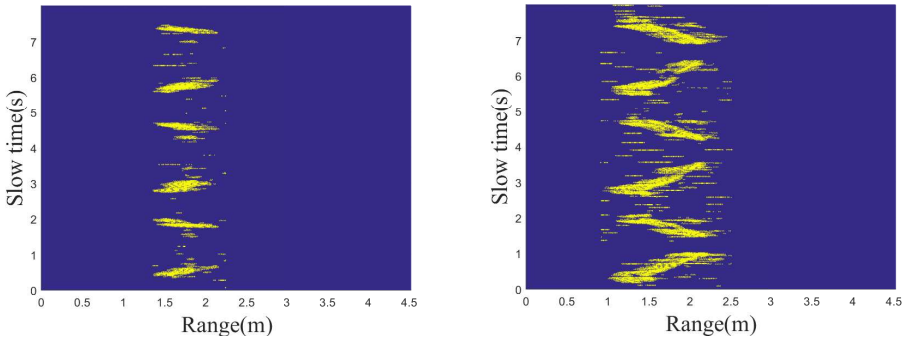

(a) The first experiment, radar 1 signal image.

(b) The first experiment, radar 2 signal image.

Figure 3.10: The first experiment radar images.

the direction angle of motion and make the motion direction as 45 degrees with respect to both of the radar boresights. Figure 3.11 demonstrate the results. The

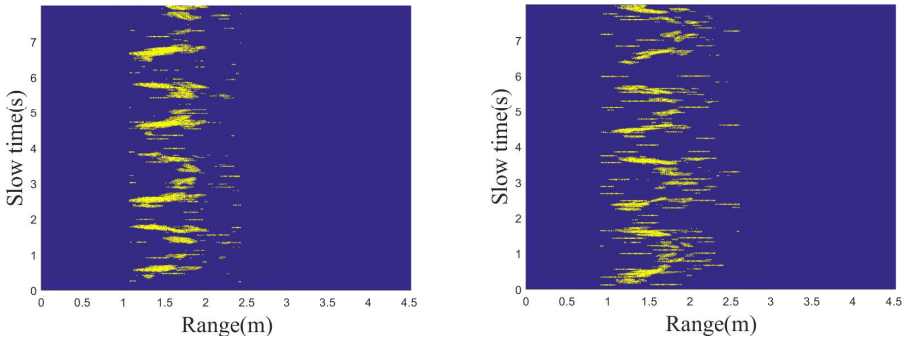

(a) The second experiment, radar 1 signal image.

(b) The second experiment, radar 2 signal image.

Figure 3.11: The second experiment radar images.

results of the second experiment show the possiblity that two radars provide similar information for the human motion.

3.2 Image Based Human Motion Feature Extraction

3.2.1 Motion History Image

The motion history image (MHI) is a static image template helps in understanding the motion location and path as it progresses. In MHI, the temporal motion information is collapsed into a single image template where intensity is a function of recency of motion. Thus, the MHI pixel intensity is a function of the motion history at that location, where brighter values correspond to a more recent motion. Using MHI, moving parts of a video sequence can be engraved with a single image, from where one can predict the motion flow as well as the moving parts of the video action. The MHI expresses the motion flow or sequence by using the intensity of every pixel in a temporal manner. Motion history image has been applied as an effective tools to describe motion shapes and spatial distributions using motion sequences that imply the recency of human actions [47]. In order to describe the motion in the image sequence, one can form an MHI of the target energy, and represent where the motion or a spatial pattern occurs. The advantages of MHI representations lie in that video images can be recoded in a single MHI frame. In this way, a small number of MHIs can span the time scale of human motions.

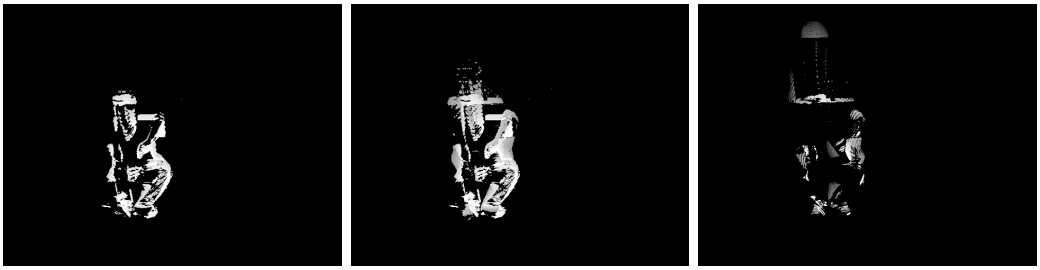

(a) τ=5 (b) τ=10 (c) τ=20

Figure 3.12: Dependence on τ to develop MHI images.

MHI $H_\tau(x, y, t)$ is given by:

$$H_\tau(x, y, t) = \begin{cases} \tau, & \text{if } D(x, y, t) = 1, \\ \max(0, H_\tau(x, y, t-1) - \delta), & \text{otherwise,} \end{cases} \tag{3.1}$$

where x and y describe the position, t is time, $D(x, y, t)$ is an update function indicating that an object is present in the current video image. In addition, τ is the duration that decides the temporal extent of the movement, and δ is the decay.

Figure 3.12 give examples of falling MHI images with three different values of τ, i.e., $\tau = 5$, $\tau = 10$ and $\tau = 20$.

3.2.2 Hu Moments

Moments have been extensively applied to characterize the image patterns [48]. In order to extract features of the segmented MHIs, eight statistic descriptors from the Hu moments, which are invariant to scale, translation and rotation, are calculated for every MHI frame $H_\tau(x, y, k)$, where k is the index of the MHI frame. A two-dimensional (2-D) $(i + j)$th order moment of the image function $f(x, y)$ is defined as:

$$m_{ij} = \int_{-\infty}^{\infty} \int_{-\infty}^{\infty} x^i y^j f(x, y) dx dy, \ i, j = 0, 1, 2... \tag{3.2}$$

If the image function is a sectional function, the moments of all orders exist and the moment sequence m_{ij} is determined by $f(x, y)$; and accordingly, $f(x, y)$ is determined by the moment sequence m_{ij}. It is noted that the moments in (2) may vary when $f(x, y)$ changes by translating, rotating or scaling. Therefore, the following central moments are used to obtain features that are invariant to image translation,

rotation and scaling:

$$\mu_{ij} = \int_{-\infty}^{\infty}\int_{-\infty}^{\infty}(x-\overline{x})^i(y-\overline{y})^j f(x,y)dxdy, i,j = 0,1,2,... \tag{3.3}$$

where $\overline{x} = m_{10}/m_{00},\ \overline{y} = m_{01}/m_{00}$. There totally 8 invariant moments up to 3 orders with i, j=0,...,3 that we consider as the features of those video clips, which are,

$$\begin{aligned}
h_1 &= \beta_{20} + \beta_{02},\\
h_2 &= (\beta_{20} - \beta_{02})^2,\\
h_3 &= (\beta_{30} - 3\beta_{12})^2 + (3\beta_{21} - \beta_{03})^2,\\
h_4 &= (\beta_{30} + \beta_{12})^2 + (\beta_{21} + \beta_{03})^2,\\
h_5 &= (\beta_{30} - 3\beta_{12})(\beta_{30} + \beta_{12})[(\beta_{30} + \beta_{12})^2 - 3(\beta_{21} + \beta_{03})^2]\\
&\quad +(3\beta_{21} - \beta 03)(\beta_{21} + \beta_{03})[3(\beta_{30} + \beta_{12})^2 - (\beta_{21} + \beta_{03})^2],\\
h_6 &= (\beta_{20} - \beta_{02})[(\beta_{30} + \beta_{12})^2 - (\beta_{21} + \beta_{03})^2] + 4\beta_{11}(\beta_{30} + \beta_{12})(\beta_{21} + \beta_{03}),\\
h_7 &= (3\beta_{21} - \beta_{02})(\beta_{30} + \beta_{12})[(\beta_{30} + \beta_{12})^2 - 3(\beta_{21} + \beta_{03})^2]\\
&\quad +(3\beta_{12} - \beta_{30})(\beta_{21} + \beta_{03})[3(\beta_{30} + \beta_{12})^2 - (\beta_{21} + \beta_{03})^2],\\
h_8 &= \beta_{11}(\beta_{30} + \beta_{12})^2 - (\beta_{03} + \beta_{21})^2\\
&\quad -(\beta_{20} - \beta_{02})(\beta_{30} + \beta_{12})(\beta_{21} + \beta_{03})
\end{aligned} \tag{3.4}$$

where $\beta_{ij} = \frac{\mu_{ij}}{\mu_{00}^{\gamma}}$ and $\gamma = \frac{i+j}{2} + 1$.

3.3 UWB Radar Based Human Motion Feature Extraction

The filtered radar signal is expressed as:

$$\mathbf{r}_k = [s_{k,2} - s_{k,1}, ..., s_{k,L} - s_{k,L-1}]^T. \tag{3.5}$$

In such case, we rebuild the filtered radar signal matrix as $R = [\mathbf{r}_1, \mathbf{r}_2, ..., \mathbf{r}_K]$. Figure 3.13 shows the filtered result for falling, and Figure 3.14 for sitting.

It is still difficult to clearly classify falling versus sitting from the filtered results as those depicted in Figure 3.13 and 3.14. In order to enhance the contrast between these motions, a threshold is set to discard the values below it. The radar image is then converted to a 2-D logical matrix

$$R_{k,l} = \begin{cases} 0, & R_{k,l} \leq Th_k, \\ 1, & \text{otherwise}, \end{cases} \tag{3.6}$$

for k=1,...,K; l=1,...,L-1.
where $Th_k = \sqrt{\frac{1}{L-1}\sum_{l=1}^{L-1} R_{k,l}^2}$ is the quadratic mean of each row, and $R_{k,l}$ is the element of matrix R. This process eliminates the influence of low reflective body scatterers which may contaminate the received signals, and forms a new radar signal matrix R with K rows and $L-1$ columns.

Signal processing is carried out based on this filtered matrix aiming at detecting moving targets and identifying the specific range between the targets and the radar. To reduce the dimension of the radar data matrix while preserving the motion characteristics, the principal component analysis (PCA) is used for dimension reduction. PCA performs an orthogonal transformation to convert radar signal R

to a new coordinate system that consists of linearly uncorrelated variables. The new variables referred to as the principal components. By choosing the first n principal components, we can reduce data dimension from $(L-1) \times K$ to $n \times K$ while preserving most of the information in R, and $(.)^H$ denotes conjugate transpose.

$$R_{(n \times K)} = A_{(n \times n)} \Lambda_{(n \times K)} B_{(K \times K)} \tag{3.7}$$

where $A_{(n \times n)}$ is an $n \times n$ matrix containing eigenvectors of covariance matrix RR^H of radar data, $\Lambda_{(n \times K)}$ is a rectangular diagonal matrix, $B_{(K \times K)}$ is the eigenvectors of $R^H R$.

In fact, we extract n eigenvalues with total cumulative over 85% under the following criteria,

$$\frac{\sum_{k=1}^{i} \lambda_k}{\sum_{k=1}^{K} \lambda_k} \geq 85\%, \ i = 1, 2, ..., K \tag{3.8}$$

where, λ_k is the kth eigenvalue of covariance matrix RR^H. In this application, we select the value of n to be 60 to satisfy the above criterion.

3.4 Time Series Data Analysis

The feature vectors from video and radar data corresponding to all the motion classes are partitioned into c clusters $S = S_1, S_2, ..., S_c$ by the k-means clustering algorithm. Figure 3.15 shows the output radar based scatter plot of falling motions whereas Figure 3.16 gives the result for sitting motions. These figures indicate that the features for these two types of motions are much better distinguished as compared with the radar imaging depicted in Figure 3.13 and 3.14.

HMMs are known for their application in temporal pattern recognition which use observable variables to learn the way of objectives. An HMM describes stochastic sequences as Markov chains where the states are related to a probability function.

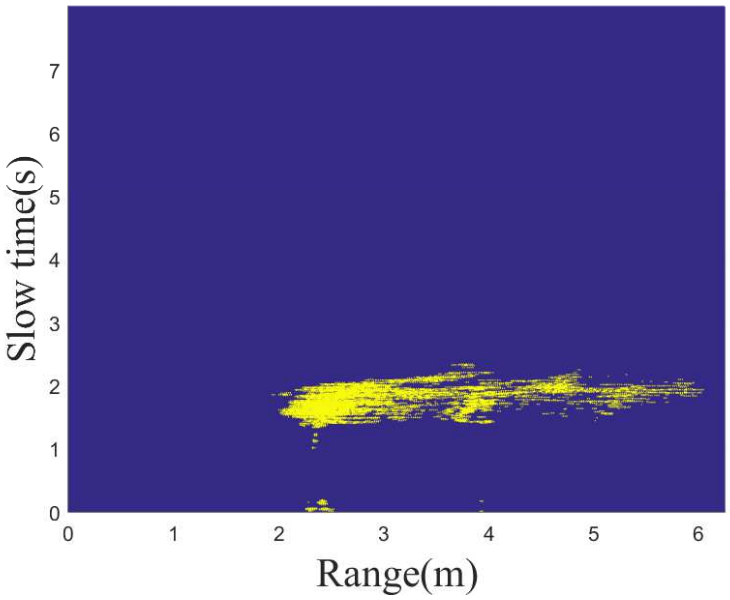

Figure 3.13: Radar detection image of falling.

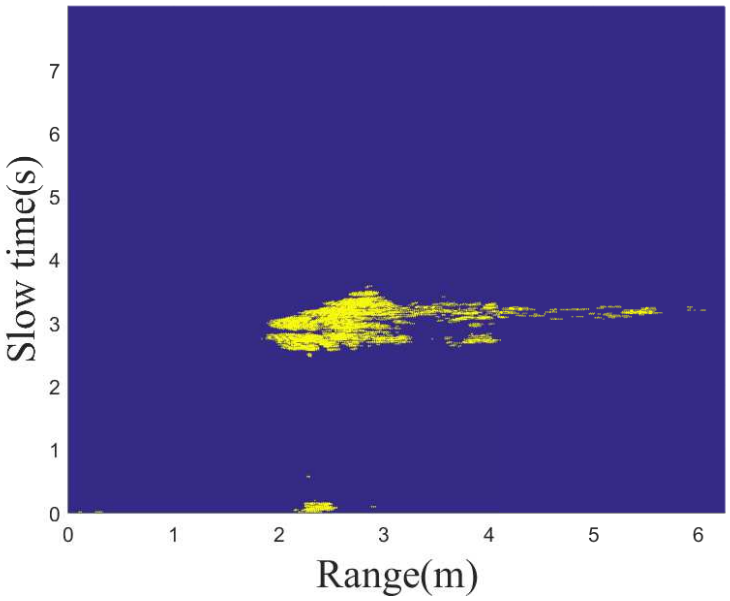

Figure 3.14: Radar detection image of sitting.

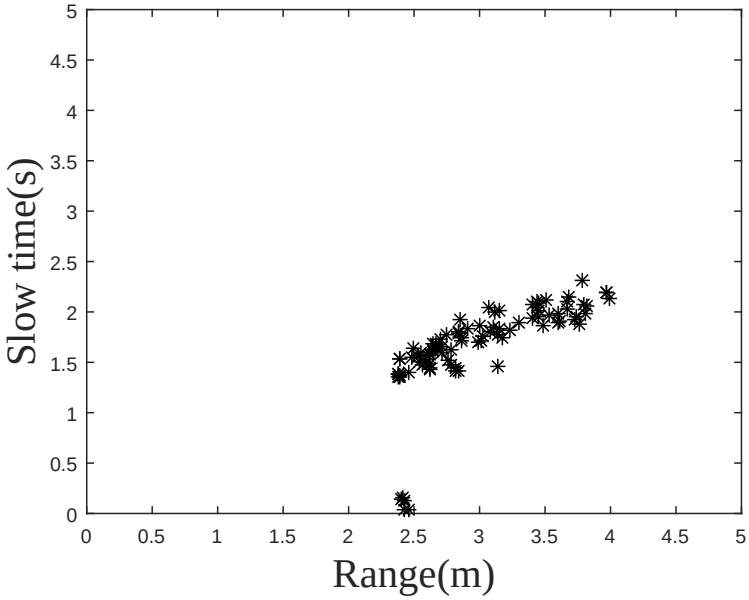

Figure 3.15: Scatter plot of falling using PCA.

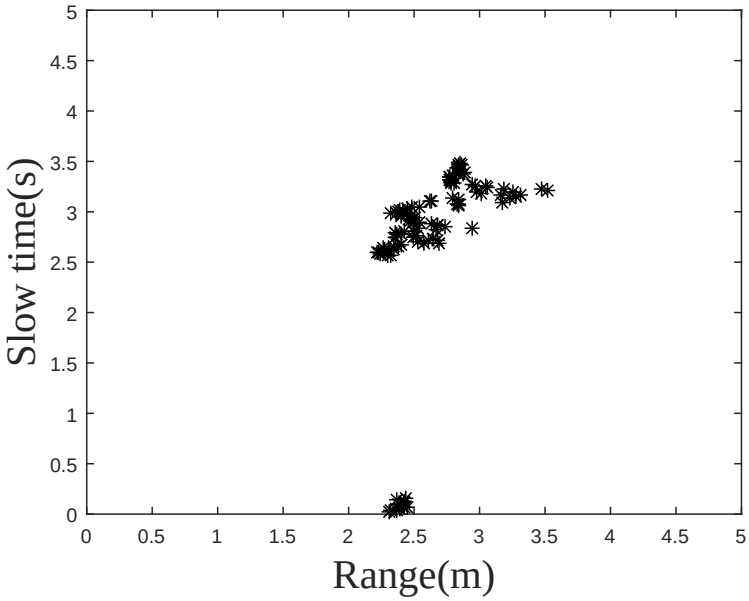

Figure 3.16: Scatter plot of sitting using PCA.

Consider an N-state HMM described as

$$\lambda = \{X,\ Y,\ \pi\}\ , \tag{3.9}$$

where X is the probability of transfering to another state q at next time $t+1$ given the current state p at current time t, Y is the probability of being observing symbol at state q. In the proposed approach, two HMM models are desinated respectively as falling and sitting models. Testing sequence ϑ is classified in model $\lambda_{\hat{i}}$, $\hat{i}$=1 (falling), 2 (sitting).

$$\hat{i} = \arg\max\ P(\vartheta|\lambda_{\hat{i}}). \tag{3.10}$$

where $P(\vartheta|\lambda_{\hat{i}})$ is the likelihood probability, and implies that the HMM-based classification based on the maximum probability.

3.5 Human Motion Classification Results

Experiments are performed for data collection in order to verify the effectiveness of the proposed approches. A Kinect sensor is used to record the RGB video images, wheras a UWB radar is used to collect radar reflections. Video and radar data collections are performed simultaneously and synchronously. In the series of experiments, the subjects fall towards the Kinect camera and the radar. There are 7 subjects for fallings and 6 subjects for sitings. Specifically, 49 falling and 47 sitting are used as training data. These data are utilized to build the two types of motion models.

3.5.1 Classification without cross validation

In order to understand the accuracy of the built models, we prepared other 27 of 60 falling and 33 sitting motions to be tested in each of the trained HMMs.

Training		Testing	
96		60	
falling	sitting	falling	sitting
49	47	27	33

Table 3.1: Selection of training and testing data

Activities	falling	sitting
falling	26	1
sitting	9	25

Table 3.2: Confusion matrix of video based approach

Activities	falling	sitting
falling	27	0
sitting	4	29

Table 3.3: Confusion matrix of radar based approach

The motion activities are listed in Table 3.1. Table 3.2 shows the result for video-based classification. 26 in 27 falling motions are correctly classified and 9 sitting motions are mis-classified. Video-based recogintion rate is 96.30% for falling detection and 75.76% for sitting detection. Table 3 shows the results obtained from the radar data that all the falling motions are classified correctly, and 29 in 33 sitting motions are successfully recognized. The radar-based recognition rate is 100% for falling and 87.88% for sitting. The results imply that the radar based approach give us a more precise recognition especially for sitting motions.

3.5.2 10-fold Cross Validation

In order to demonstrate the confidence of the classification models, cross validation has also been implemented for training and testing. All data have been randomly grouped into ten folds, we run 10 separate learning experiments in total to evaluate the recognition accuracy rates. For each experiments, we use 9 folds for training and the remaining one for testing.

Table 3.4: 10-fold cross validation based video approach classification results

		Fall	Sit	Fall Recognition Rate	Sit Recognition Rate
Group 1	Fall	9	1	90.00%	85.71%
	Sit	1	6		
		Fall	Sit		
Group 2	Fall	6	1		87.50%
	Sit	1	7		
		Fall	Sit		
Group 3	Fall	6	0	100.00%	88.89%
	Sit	1	8		
		Fall	Sit		
Group 4	Fall	7	0	100.00%	87.50%
	Sit	1	7		
		Fall	Sit		
Group 5	Fall	5	0	100.00%	81.82%
	Sit	2	9		
		Fall	Sit		
Group 6	Fall	6	1	85.71%	75.00%
	Sit	2	6		
		Fall	Sit		
Group 7				80.00%	70.00%

	Fall	4	1		
	Sit	3	7		
Group 8		Fall	Sit	100.00%	87.5%
	Fall	8	0		
	Sit	1	7		
Group 9		Fall	Sit	83.33%	80.00%
	Fall	10	2		
	Sit	1	4		
Group 10		Fall	Sit	81.81%	100.00%
	Fall	9	2		
	Sit	0	6		
Average Accuracy				90.66%	84.39%

Table 3.4 provides the confusion matrix and recognition rates for all 10 cross-validation experiments in video based approach. The classification accuracy is estimated as the average which are 90.66% and 84.39%, respectively. The average rates show that, compare with results in Table 3.2, the fall motion recognition accuracy drops from 96.30% to 90.66%, and the sit motion recognition rate increases to 84.39%.

Table 3.5: 10-fold cross validation based radar approach classification results

		Fall	Sit	Fall Recognition Rate	Sit Recognition Rate
Group 1	Fall	10	0	100.00%	85.71%
	Sit	1	6		
Group 2		Fall	Sit	85.71%	100.00%
	Fall	6	1		
	Sit	0	8		

Group 3		Fall	Sit	100.00%	88.89%
	Fall	6	0		
	Sit	1	8		
Group 4		Fall	Sit	100.00%	75.00%
	Fall	7	0		
	Sit	2	6		
Group 5		Fall	Sit	100.00%	90.91%
	Fall	5	0		
	Sit	1	10		
Group 6		Fall	Sit	85.71%	87.50%
	Fall	6	1		
	Sit	1	7		
Group 7		Fall	Sit	100.00%	80.00%
	Fall	5	0		
	Sit	2	8		
Group 8		Fall	Sit	100.00%	100.00%
	Fall	8	0		
	Sit	0	8		
Group 9		Fall	Sit	83.33%	80.00%
	Fall	10	2		
	Sit	1	4		
Group 10		Fall	Sit	100.00%	100.00%
	Fall	11	0		
	Sit	0	6		
Average Accuracy				95.48%	88.80%

Comparing with Table 3.3, which shows that the recognition rate for falling is as high as 100%, the average accuracy given by Table 3.5 shows a more convincing result at 95.48%. Meanwhile, the accuracy for classifying sit motion has improved from 87.88% to 88.80%.

Chapter 4

Conclusion

The goal of this thesis project is to use UWB radar to realize human body landmark detection and human motion classification. The research work presented in this thesis proposes a UWB radar based landmark and multi-target detection approach for accurate human motion measuring. An out-of-band (OB) CFAR method is proposed to detect the human body landmarks. Comparing with the conventional CFAR method, our OB-CFAR shows better performance in detecting the reflectors.

This thesis also investigated the classification and recognition of human motions using camera and UWB radar based sensing modalities, respectively. We utilized the MHI and Hu moment methods to extract features of RGB images. For radar data, we applied motion filtering and PCA to reduce the data dimension and extract the features. The k-means clustering algorithm is utilized for vector quantization. Two HMMs for falling and sitting motions are trained for vision based and radar based data, respectively. From the classification results, we observed that the radar based method achieves higher classification performance with recognition rate of 95.48% in falling and 88.80% in sitting. This comparison successfully implies the advantages of UWB radar based human motion classification. Then we implement the 10 fold cross-validation method on training and testing. The results show more

confident and accurate classification rates which also indicate that the methodologies we applie on feature extracting and classification are feasible.

Bibliography

[1] Wai Yin Wong, Man Sang Wong, and Kam Ho Lo. Clinical Applications of Sensors for Human Posture and Movement Analysis: a review. *Prosthetics and orthotics international*, 31(1):62–75, 2007.

[2] Quanhua Liu, Yazhou Wang, and Aly E Fathy. A Compact Integrated 100 GS/s Sampling Module for UWB See Through Wall Radar with Fast Refresh Rate for Dynamic Real Time Imaging. In *Radio and Wireless Symposium (RWS), IEEE*, pages 59–62. IEEE, 2012.

[3] Piljae Park, Sungdo Kim, Sungchul Woo, and Cheonsoo Kim. A High-resolution Short-range CMOS Impulse Radar for Human walk Tracking. In *Radio Frequency Integrated Circuits Symposium (RFIC), IEEE*, pages 9–12. IEEE, 2013.

[4] VE Ivashchuk, VP Prokhorenko, AA Pitertsev, and FJ Yanovsky. Evaluation of combined ground penetrating and Through-the-Wall Surveillance UWB technology. In *Microwave Conference (EuMC), European*, pages 384–387. IEEE, 2013.

[5] B Levitas, J Matuzas, and M Drozdov. Detection and Separation of Several Human Beings Behind the Wall with UWB Radar. In *International Radar Symposium*, 2008.

[6] Jing Li, Zhaofa Zeng, Jiguang Sun, and Fengshan Liu. Through-wall Detection of Human Being's Movement by UWB Radar. *Geoscience and Remote Sensing Letters, IEEE*, 9(6):1079–1083, 2012.

[7] Shobha Sundar Ram, Craig Christianson, and Hao Ling. Simulation of High Range-resolution Profiles of Humans behind Walls. In *IEEE Radar Conference*, 2009.

[8] Martin Safarik, Jan Mrkvica, Pavel Protiva, and Radim Sikl. Three-dimensional Image Fusion of Moving Human Target Data Measured by a Portable Through-wall Radar. In *Radioelektronika (RADIOELEKTRONIKA), 23rd International Conference*, pages 308–311. IEEE, 2013.

[9] Shiyou Wu, Kai Tan, Yanyun Xu, Jie Chen, Shengwei Meng, and Guangyou Fang. A Simple Strategy for Moving Target Imaging via an Experimental UWB Through-wall Radar. In *Ground Penetrating Radar (GPR), 14th International Conference on*, pages 961–965. IEEE, 2012.

[10] Guofu Zhu, Jun Hu, Zhenlong Yuan, and Xiaotao Huang. Automatic Human Target Detection of Ultra-wideband Through-wall Radar. In *Radar Conference (RADAR), IEEE*, pages 1–4. IEEE, 2013.

[11] Bernd Schleicher, Jochen Dederer, Mario Leib, Ismail Nasr, Andreas Trasser, Wolfgang Menzel, and Hermann Schumacher. Highly Compact Impulse UWB Transmitter for High-resolution Movement Detection. In *Ultra-Wideband. ICUWB. IEEE International Conference on*, volume 1, pages 89–92. IEEE, 2008.

[12] Bernd Schleicher, Ismail Nasr, Andreas Trasser, and Hermann Schumacher. IR-UWB Radar Demonstrator for Ultra-fine Movement Detection and Vital-sign Monitoring. *Microwave Theory and Techniques, IEEE Transactions on*, 61(5):2076–2085, 2013.

[13] Nadia Maaref, Patrick Millot, Ch Pichot, and Odile Picon. A Study of UWB FM-CW Radar for the Detection of Human Beings in Motion inside a Building. *Geoscience and Remote Sensing, IEEE Transactions on*, 47(5):1297–1300, 2009.

[14] Enrico M Staderini. UWB Radars in Medicine. *Aerospace and Electronic Systems Magazine, IEEE*, 17(1):13–18, 2002.

[15] I Immoreev and S Ivashov. Remote Monitoring of Human Cardiorespiratory System Parameters by Radar and Its Applications. In *Ultrawideband and Ultrashort Impulse Signals, UWBUSIS. 4th International Conference on*, pages 34–38. IEEE, 2008.

[16] F Thiel and F Seifert. Noninvasive Probing of the Human Body with Electromagnetic Pulses: Modeling of the signal path. *Journal of Applied Physics*, 105(4):044904, 2009.

[17] Anatoliy Boryssenko and Elen Boryssenko. UWB Radar Sensor to Monitor Heart Physiology. In *Antennas and Propagation Conference (LAPC), Loughborough*, pages 1–4. IEEE, 2011.

[18] Ta-Shun Chu, Jonathan Roderick, SangHyun Chang, Timothy Mercer, Chenliang Du, and Hossein Hashemi. A Short-range UWB Impulse-radio CMOS Sensor for Human Feature Detection. In *Solid-State Circuits Conference Digest of Technical Papers (ISSCC), IEEE International*, pages 294–296. IEEE, 2011.

[19] Yazhou Wang, Quanhua Liu, and Aly E Fathy. Simultaneous Localization and Respiration Detection of Multiple People using Low Cost UWB Biometric Pulse Doppler Radar Sensor. In *Microwave Symposium Digest (MTT), IEEE MTT-S International*, pages 1–3. IEEE, 2012.

[20] Yogesh Nijsure, Wee Peng Tay, Erry Gunawan, Fuxi Wen, Zhang Yang, Yong Liang Guan, and Ai Ping Chua. An Impulse Radio Ultrawideband System for Contactless Noninvasive Respiratory Monitoring. *Biomedical Engineering, IEEE Transactions on*, 60(6):1509–1517, 2013.

[21] Sheldon R Simon. Quantification of Human Motion: Gait analysisbenefits and limitations to its application to clinical problems. *Journal of biomechanics*, 37(12):1869–1880, 2004.

[22] Yazhou Wang and Aly E Fathy. Micro-Doppler Signatures for Intelligent Human Gait Recognition using a UWB Impulse Radar. In *Antennas and Propaga-*

tion (APSURSI), IEEE International Symposium on, pages 2103–2106. IEEE, 2011.

[23] Jacob Bryan and Youngwook Kim. Classification of Human Activities on UWB Radar using a Support Vector Machine. In *Antennas and Propagation Society International Symposium (APSURSI), IEEE*, pages 1–4. IEEE, 2010.

[24] JD Bryan, Joonsoo Kwon, Namyoon Lee, and Youngjae Kim. Application of Ultra-wide Band Radar for Classification of Human Activities. *Radar, Sonar & Navigation, IET*, 6(3):172–179, 2012.

[25] Kenshi Saho, Takuya Sakamoto, Toru Sato, Kenichi Inoue, and Takeshi Fukuda. Pedestrian Classification Based on Radial Velocity Features of UWB Doppler Radar Images. In *Antennas and Propagation (ISAP), International Symposium on*, pages 90–93. IEEE, 2012.

[26] Takanori Sakamoto, Takao Sato, Yuan He, Pascal J Aubry, and Alexander G Yarovoy. Texture-based Technique for Separating Echoes from People Walking in UWB Radar Signals. In *Electromagnetic Theory (EMTS), Proceedings of URSI International Symposium on*, pages 119–122. IEEE, 2013.

[27] Kenshi Saho, Takuya Sakamoto, and Toru Sato. Imaging of Pedestrians with UWB Doppler Radar Interferometry. In *Proc. of*, pages 29–32, 2013.

[28] Yazhou Wang and Aly E Fathy. Three-dimensional Through Wall Imaging using an UWB SAR. In *Antennas and Propagation Society International Symposium (APSURSI), IEEE*, pages 1–4. IEEE, 2010.

[29] Arpit Gupta, Vidit Saxena, and Sachin Joshi. Development of a High Resolution UWB Sensor for Estimation of Transfer Function of Vocal Tract Filter. In *Wireless Communication and Sensor Networks. WCSN'07. Third International Conference on*, pages 131–134. IEEE, 2007.

[30] Teh-Ho Tao, Shin-Jen Hu, Jla-Hung Peng, and Su-Chen Kuo. An Ultra-wideband Radar Based Pulse Sensor for Arterial Stiffness Measurement. In *Engineering in Medicine and Biology Society, 2007. EMBS 2007. 29th Annual International Conference of the IEEE*, pages 1679–1682. IEEE, 2007.

[31] Mohamed AA Eldosoky. The Applications of the Ultra Wide Band Radar in Detecting the Characteristics of the Human Arm Muscles. In *Radio Science Conference, NRSC. National*, pages 1–7. IEEE, 2009.

[32] Sevgi Zübeyde Gürbüz. Radar Detection and Identification of Human Signatures using Moving Platforms. 2009.

[33] Liang Liu, Mihail Popescu, KC Ho, Marjorie Skubic, and Marilyn Rantz. Doppler Radar Sensor Positioning in a Fall Detection System. In *Proceedings of Annual International Conference of the IEEE Engineering in Medicine and Biology Society (EMBC)*, pages 256–259, San Diego, CA, 2012.

[34] Meng Wu, Xiaoxiao Dai, Yimin D Zhang, Bradley Davidson, Moeness G Amin, and Jun Zhang. Fall Detection Based on Sequential Modeling of Radar Signal Time-frequency Features. In *Proceedings of IEEE International Conference on Healthcare Informatics (ICHI)*, pages 169–174, 2013.

[35] Moeness G Amin, Yimin D Zhang, Fauzia Ahmad, and KC Dominic Ho. Radar Signal Processing for Elderly Fall Detection: The future for in-home monitoring. *IEEE Signal Processing Magazine*, 33(2):71–80, 2016.

[36] T. R. Bennett, J. Wu, N. Kehtarnavaz, and R. Jafari. Inertial Measurement Unit-Based Wearable Computers for Assisted Living Applications: A signal processing perspective. *IEEE Signal Processing Magazine*, 33(2):28–35, March 2016.

[37] Xiangcun Wang, Min Li, Houwei Ji, and Zhenbang Gong. A Novel Modeling Approach to Fall Detection and Experimental Validation using Motion Capture System. In *Proceedings of IEEE International Conference on Robotics and Biomimetics (ROBIO)*, pages 234–239, 2013.

[38] Yun Li, KC Ho, and Mihail Popescu. Efficient Source Separation Algorithms for Acoustic Fall Detection using a Microsoft Kinect. *IEEE Transactions on Biomedical Engineering*, 61(3):745–755, 2014.

[39] Sanaz Kianoush, Stefano Savazzi, Federico Vicentini, Vittorio Rampa, and Matteo Giussani. Leveraging RF signals for human sensing: fall detection and localization in human-machine shared workspaces. In *Proceedings of IEEE 13th International Conference on Industrial Informatics (INDIN)*, pages 1456–1462, 2015.

[40] Anthony Martone, Kenneth Ranney, and Roberto Innocenti. Automatic through the Wall Detection of Moving Targets using Low-frequency Ultra-wideband Radar. In *Proceedings of IEEE Radar Conference*, pages 39–43, 2010.

[41] Jun Hao, Xiaoxiao Dai, Amy Stroder, Jun Jason Zhang, Bradley Davidson, Mohammad Mahoor, and Neil McClure. Prediction of a Bed-exit motion: Multimodal Sensing Approach and Incorporation of Biomechanical Knowledge. In *Proceedings of 48th Asilomar Conference on Signals, Systems and Computers*, pages 1747–1751, 2014.

[42] Zafer Sahinoglu, Sinan Gezici, and Guvenc Ismail. *Ultra-wideband Positioning Systems: Theoretical Limits, Ranging Algorithms, and Protocols*. Cambridge University Press, 2008.

[43] Camillo Gentile and Alfred Kik. A Comprehensive Evaluation of Indoor Ranging using Ultra-wideband Technology. *EURASIP Journal on Wireless Communications and Networking*, 2007(1):12–12, 2007.

[44] AG Yarovoy, LP Ligthart, J Matuzas, and B Levitas. UWB radar for human being detection. *IEEE Aerospace and Electronic Systems Magazine*, 21(3):10–14, 2006.

[45] Hamish Meikle. *Modern Radar Systems*. Artech House, 2008.

[46] Fok Ring Chi Tivive, Abdesselam Bouzerdoum, and Moeness G Amin. Automatic Human Motion Classification from Doppler Spectrograms. In *Cognitive Information Processing (CIP), 2nd International Workshop on*, pages 237–242. IEEE, 2010.

[47] Md Atiqur Rahman Ahad, JK Tan, H Kim, and S Ishikawa. Human Activity Analysis: Concentrating on Motion History Image and Its Variants. In *ICCAS-SICE*, pages 5401–5406. IEEE, 2009.

[48] Zhihu Huang and Jinsong Leng. Analysis of Hu's Moment Invariants on Images Scaling and Rotation. In *2nd International Conference on Computer Engineering and Technology*, pages 476–480, 2010.